

Supplementary Information for

Photoreductive Chlorine Elimination from a Ni(III)Cl₂ Complex Supported by a Tetradentate Pyridinophane Ligand

Hanah Na,^a Michael B. Watson,^b Fengzhi Tang,^b Nigam P. Rath,^c and Liviu M. Mirica^{*a}

^aDepartment of Chemistry, University of Illinois at Urbana-Champaign, Urbana, Illinois, 61801

^bDepartment of Chemistry, Washington University, St. Louis, Missouri, 63130

^cDepartment of Chemistry and Biochemistry, University of Missouri – St. Louis, St. Louis, Missouri, 63121

*E-mail: mirica@illinois.edu

Contents

1. General specifications	S2
2. Synthesis	S3
3. Cyclic voltammograms of the ^{Me} N ₄ Ni ^{II} Cl ₂ complex (1)	S4
4. Electron paramagnetic resonance (EPR) experiments	S5
5. UV-vis absorption spectra.....	S7
6. UV-vis absorption spectra of 1 with irradiation	S8
7. Paramagnetic ¹ H NMR spectra	S9
7. UV-vis absorption spectra of 2 ⁺ after addition of PhICl ₂	S12
9. Quantum yield measurement for the photolysis of 1 ⁺	S13
10. Solid-state photolysis	S14
11. PBN spin trapping EPR study.....	S19
12. X-ray structure characterization.....	S20
13. Computational details	S30
14. References.....	S40

1. General specifications

Materials. Reactions were performed in ambient conditions unless otherwise stated. Solvents were purified prior to use by passing through a column of activated alumina using an M Braun solvent purification system. All starting materials and reagents, unless otherwise specified, were obtained from commercial sources and used without further purification.

Physical Methods. ^1H and NMR spectra were recorded using a Bruker 500 MHz spectrometer. UV-vis absorption spectra were recorded in MeCN in 1 cm quartz cuvettes using a Varian Cary 60 spectrophotometer. EPR spectra were recorded on a Bruker 10" EMXPlus X-band Continuous Wave EPR spectrometer at 77 K. EPR spectra simulation and analysis were performed using Bruker WINEPR SimFonia program, version 1.25. The magnetic moment was calculated via the Evan's method using a known concentration of the metal complex with a sealed capillary with the NMR solvent.^{1,2} Elemental analysis was carried out by the Microanalysis Laboratory at UIUC using an Exeter Analytical-Model CE440 CHN Analyzer. Cyclic voltammetry (CV) experiments were performed with a CHI 660D Electrochemical Analyzer using a three-electrode system in a nitrogen-filled glove box. A 3 mm diameter glassy-carbon electrode, a Pt wire, and a Ag wire were used as working electrode, counter electrode, and pseudoreference electrode, respectively. Measurements were carried out in acetonitrile solution with 0.1 M TBAPF₆ as a supporting electrolyte at scan rate of 0.1 V/s. Ferrocene was used as an internal standard, and potentials were referenced to the ferrocene/ferrocenium couple.

2. Synthesis

Reactions were performed in ambient conditions unless otherwise stated. Solvents were purified prior to use by passing through a column of activated alumina using an MBraun solvent purification system. All starting materials and reagents, unless otherwise specified, were obtained from commercial sources and used without further purification. The oxidant PhICl_2^3 and thianthrenyl tetrafluoroborate⁴ were synthesized as previously reported. The ligand N,N' -Dimethyl-2,1,1-diaza[3,3](2,6)pyridinophane ($^{\text{Me}}\text{N}_4$)⁵ was also synthesized as previously reported.

Synthesis of Ni complexes

Preparation of $^{\text{Me}}\text{N}_4\text{Ni}^{\text{II}}\text{Cl}_2$, **1**

Inside a glovebox, $^{\text{Me}}\text{N}_4$ (100 mg, 1 equiv) and $(\text{DME})\text{NiCl}_2$ (81 mg, 1 equiv) were added to a flask as solids then CH_2Cl_2 (20 mL) was added to the solids. The reaction mixture was stirred overnight. The resulting solution was filtered, and the filtrate was set up for recrystallization by diethyl ether diffusion. Yield: 129 mg (88%). ^1H NMR (CD_3CN), δ (ppm): 12.7 (br), 56.9 (br). Evans method (CH_2Cl_2): $\mu_{\text{eff}} = 3.01 \mu_{\text{B}}$. Elemental analysis: found C 48.40, H 4.82, N 13.69 %; calculated $\text{C}_{16}\text{H}_{20}\text{Cl}_2\text{N}_4\text{Ni}$, C 48.29, H 5.07, N 14.08 %.

Preparation of $[^{\text{Me}}\text{N}_4\text{Ni}^{\text{III}}\text{Cl}_2]\text{BF}_4$, [**1**] BF_4

Inside a glovebox, $^{\text{Me}}\text{N}_4\text{Ni}^{\text{II}}\text{Cl}_2$ (**1**) (50 mg, 1 equiv) was dissolved in 5 mL of CH_2Cl_2 . The solution was cooled to -35°C and a solution of thianthrene cation radical tetrafluoroborate (38 mg, 1 equiv) in 2 mL CH_2Cl_2 was added while stirring. The reaction was stirred for 1 hour at -35°C then the solution was concentrated to ~ 1 mL and diethyl ether was added to precipitate the complex. The precipitate was filtered off, washed with Toluene and ether, and dried under high vacuum. Yield: 42 mg (69%). A suitable crystal for X-ray crystallography was grown using a PF_6 salt of 1^+ . Compound [**1**] BF_4 is not NMR active. Evans method (CH_2Cl_2): $\mu_{\text{eff}} = 2.13 \mu_{\text{B}}$. Elemental analysis: found C, 39.69; H, 4.20; N, 11.27 %; calculated $\text{C}_{16}\text{H}_{20}\text{BCl}_2\text{F}_4\text{N}_4\text{Ni}$, C, 39.64; H, 4.16; N, 11.56 %.

Preparation of $[^{\text{Me}}\text{N}_4\text{Ni}^{\text{II}}\text{Cl}(\text{NCMe})]\text{PF}_6$, [**2**] PF_6

Inside of a glove box, $^{\text{Me}}\text{N}_4\text{Ni}^{\text{II}}\text{Cl}_2$ (**1**) (20 mg, 1 equiv) was dissolved in CH_3CN (2 mL) and KPF_6 (9.2 mg, 1 equiv) was added. The reaction was stirred for 1 hour then the solution was filtered through celite. Resulting solution was dried, and pale blue solids was redissolved in CH_2Cl_2 and

diethyl ether was added to precipitate the complex. The precipitate was filtered off, washed with diethyl ether, and the crude product was purified by recrystallization by diethyl ether diffusion in to the CH_2Cl_2 solution at -35°C . A suitable crystal for X-ray crystallography was grown in the presence of MeOH in the CHCl_3 solution of $[\mathbf{2}]\text{PF}_6$. Yield: 22 mg (79 %). ^1H NMR (CD_3CN), δ (ppm): 12.2 (br), 59.0 (br), 77.5 (br), 107.9 (br). Elemental analysis: found C, 38.96; H, 4.30; N, 10.79 %; calculated $\text{C}_{18}\text{H}_{23}\text{ClF}_6\text{N}_5\text{Ni}\cdot\text{CH}_2\text{Cl}_2\cdot 0.5\text{Et}_2\text{O}$, C, 39.44; H, 4.73; N, 10.95 %.

3. Cyclic voltammograms of the $^{\text{Me}}\text{N}_4\text{Ni}^{\text{II}}\text{Cl}_2$ complex (**1**)

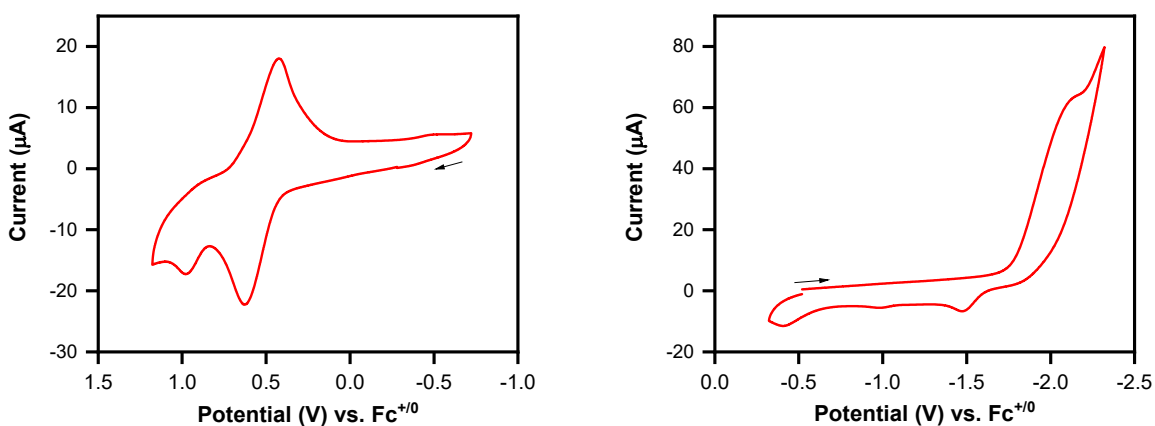


Figure S1. Cyclic voltammograms of $^{\text{Me}}\text{N}_4\text{Ni}^{\text{II}}\text{Cl}_2$ (**1**), recorded at room temperature in 0.1 M TBAPF₆/MeCN, with a scan rate of 0.1 V/s.

4. Electron paramagnetic resonance (EPR) experiments

A solution of **1** in MeCN was prepared in a glovebox at $-30\text{ }^{\circ}\text{C}$. A PrCN solution containing 1 equivalent of thianthrene cation radical tetrafluoroborate was then added while still cold. The resulting solution of 1:3 MeCN/PrCN was mixed and transferred to an EPR tube where it was frozen in liquid nitrogen and spectra were then collected.

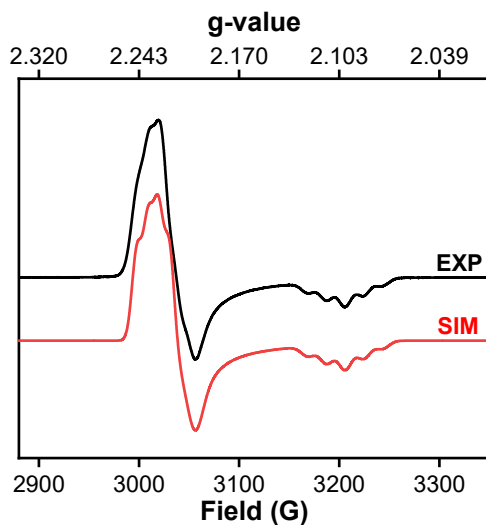


Figure S2. EPR spectrum of $[\text{MeCN}_4\text{Ni}^{\text{III}}\text{Cl}_2]\text{BF}_4$ (**[1]** BF_4) recorded at 77 K in 1:3 MeCN:PrCN.

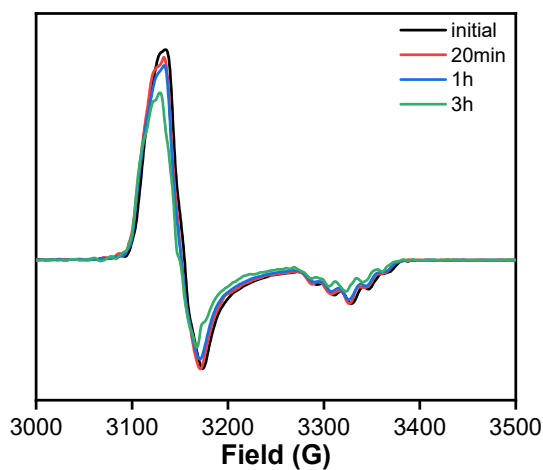


Figure S3. EPR spectra of $[\text{MeCN}_4\text{Ni}^{\text{III}}\text{Cl}_2]\text{BF}_4$ (**[1]** BF_4) stored at room temperature solution up to 3 h, showing minimal signal decay. Spectra are recorded at 77 K in 1:3 MeCN:PrCN.

EPR experiment of the regeneration of 1^+ with [thianthrene]BF₄ in the presence of TEACl

In the EPR tube, solution of 2^+ (2 mg, 1 equiv) and tetraethylammonium chloride (TEACl, 3 mg, 5 equiv) in MeCN:PrCN (1:3) was added and it was frozen in liquid nitrogen. The solution of [thianthrene]BF₄ (1.3 mg, 1 equiv) in MeCN:PrCN (1:3) was added in to the EPR tube, and the mixture was quickly mixed, and frozen in liquid nitrogen to collect spectrum at 77 K.

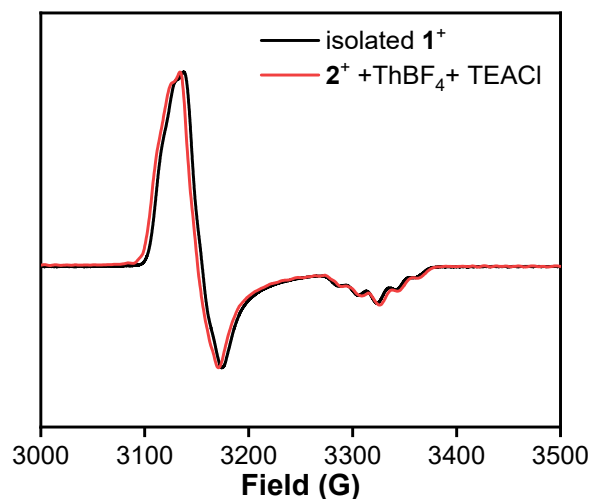


Figure S4. Overlaid EPR spectra of the reaction mixture of 2^+ with [thianthrene]BF₄ in the presence of TEACl, and isolated 1^+ [^{Me}N₄Ni^{III}Cl₂]⁺, indicating regeneration of 1^+ . Spectra are recorded at 77 K in 1:3 MeCN:PrCN.

5. UV-vis absorption spectra

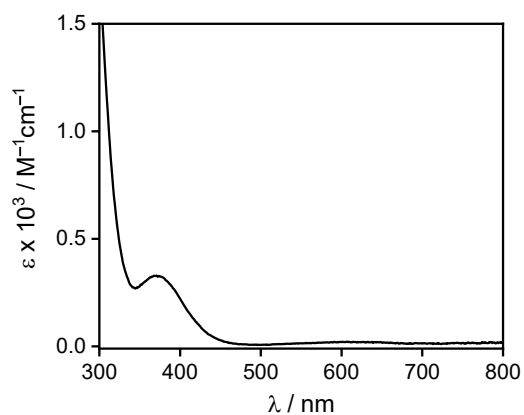


Figure S5. UV-vis absorption spectrum of $[\text{MeN}_4\text{Ni}^{\text{II}}]\text{Cl}_2$ (**1**) in CH_3CN

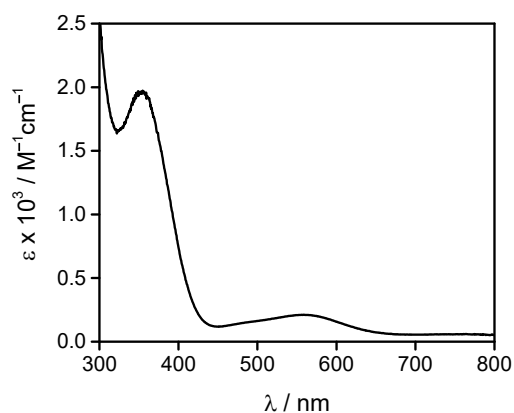


Figure S6. UV-vis absorption spectrum of $[\text{MeN}_4\text{Ni}^{\text{III}}]\text{Cl}_2[\text{BF}_4]$ (**1**) in CH_3CN

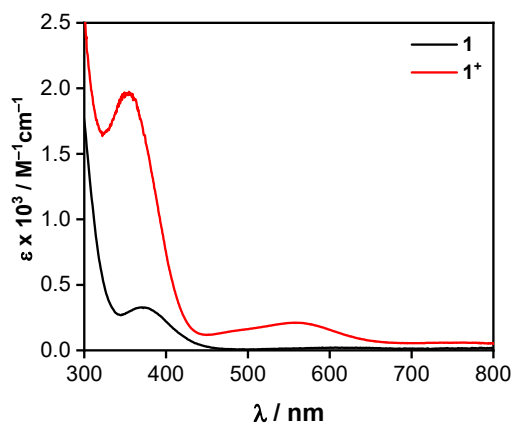


Figure S7. Overlaid UV-vis absorption spectra of $[\text{MeN}_4\text{Ni}^{\text{II}}]\text{Cl}_2$ (**1**) and $[\text{MeN}_4\text{Ni}^{\text{III}}]\text{Cl}_2[\text{BF}_4]$ (**1**) (red solid line)

6. UV-vis absorption spectra of **1** with irradiation

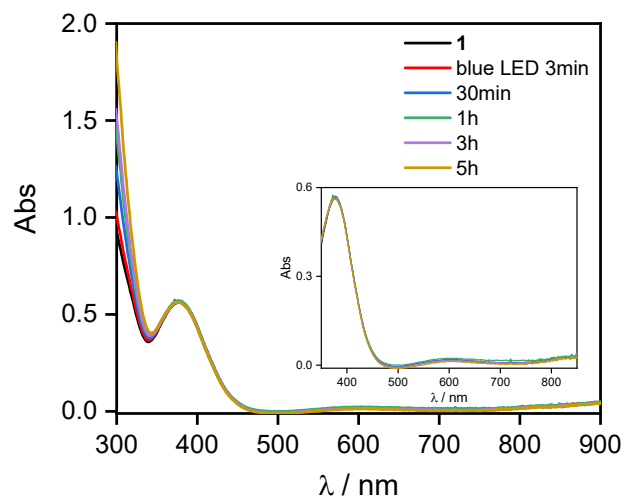


Figure S8. Photolysis of CH₃CN solution of **1** with 456 nm blue LED irradiation, showing a minimal spectral change.

7. Paramagnetic ^1H NMR spectra

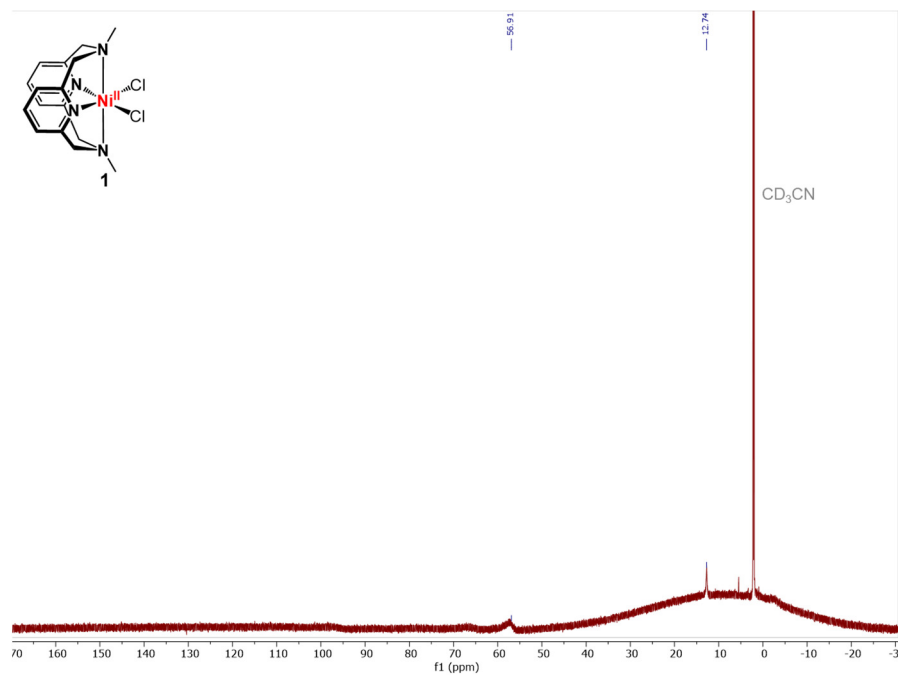


Figure S9. ^1H NMR spectrum of **1**, recorded in CD_3CN at 500 MHz.

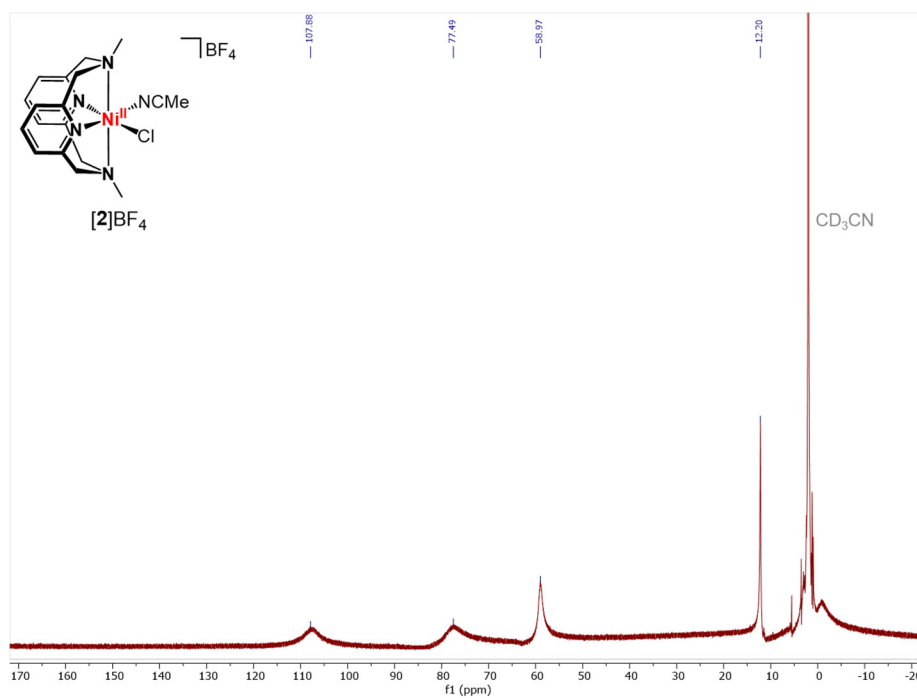


Figure S10. ^1H NMR spectrum of $[\mathbf{2}]\text{PF}_6$, recorded in CD_3CN at 500 MHz.

Photolysis experiment of [1]BF₄ for quantification of the photoreduced product [2]BF₄

Compound [1]BF₄ (5 mg, 0.01 mmol) was dissolved in 0.4 mL of CD₃CN and transferred into the NMR tube. In the NMR tube, 0.1 mL of stock solution of 1,2-dimethoxyethane in CD₃CN (1,2-dimethoxyethane 0.01 mmol, 1 equiv) was added (stock solution prepared: 11 μL of 1,2-dimethoxyethane in 1 mL of CD₃CN) as an internal standard to obtain ¹H NMR spectrum. As **1**⁺ is NMR inactive, no chemical shifts from Ni complexes were observed in the ¹H NMR spectrum. Then the NMR tube was irradiated with blue LED for 90 min. As a separate sample, independently synthesized **2**⁺ (5.6 mg, 0.01 mmol) was dissolved in 0.4 mL of CD₃CN and 0.1 mL of stock solution of 1,2-dimethoxyethane in CD₃CN as an internal standard. After mixing the solution, ¹H NMR spectrum was collected. As the compound exhibits paramagnetic shifts, the most well-resolved peaks at the upfield (12.2 ppm) of the irradiated sample and isolated **2**⁺ were integrated relative to the peaks of 1,2-dimethoxyethane. The amount of **2**⁺ generated was calculated to be 89% (Figure S12).

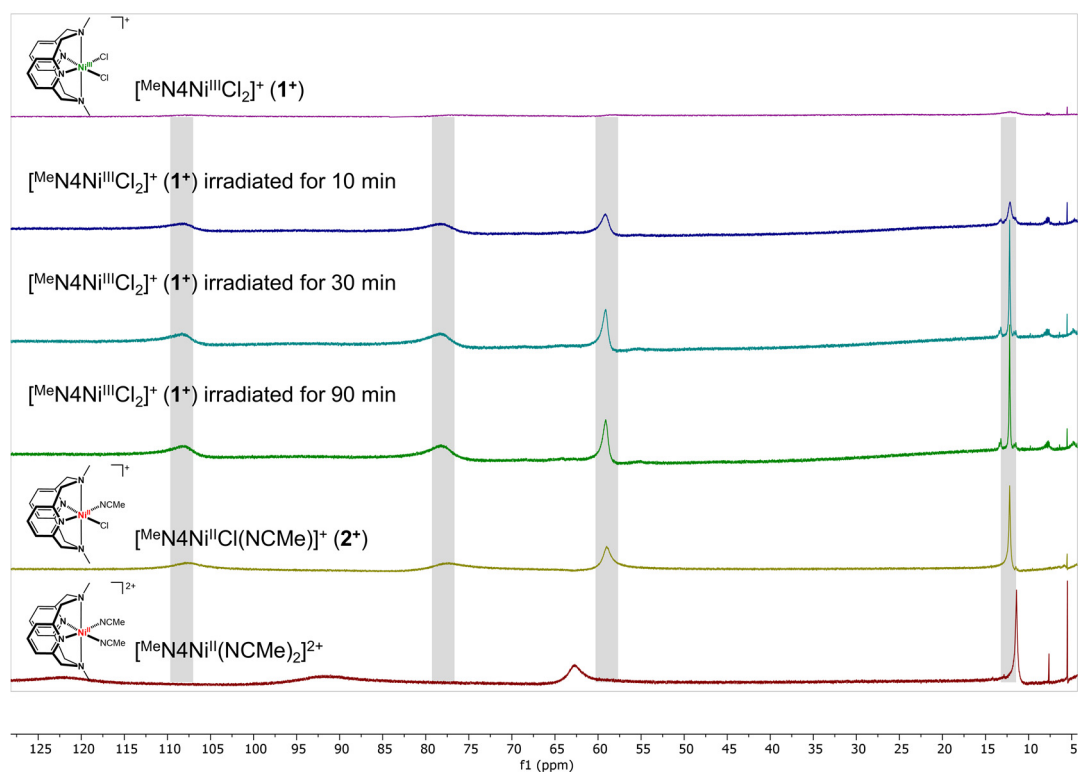


Figure S11. Stacked full paramagnetic ¹H NMR spectra of **1**⁺ during photolysis (purple, dark blue, blue, and green), and independently synthesized **2**⁺ (olive) and [MeN₄Ni^{II}(NCMe)₂]²⁺ (red), confirming the identity of the photoreduction product. The compound **1**⁺ is NMR inactive. All spectra were recorded at 500 MHz and referenced to the CD₃CN solvent peak.

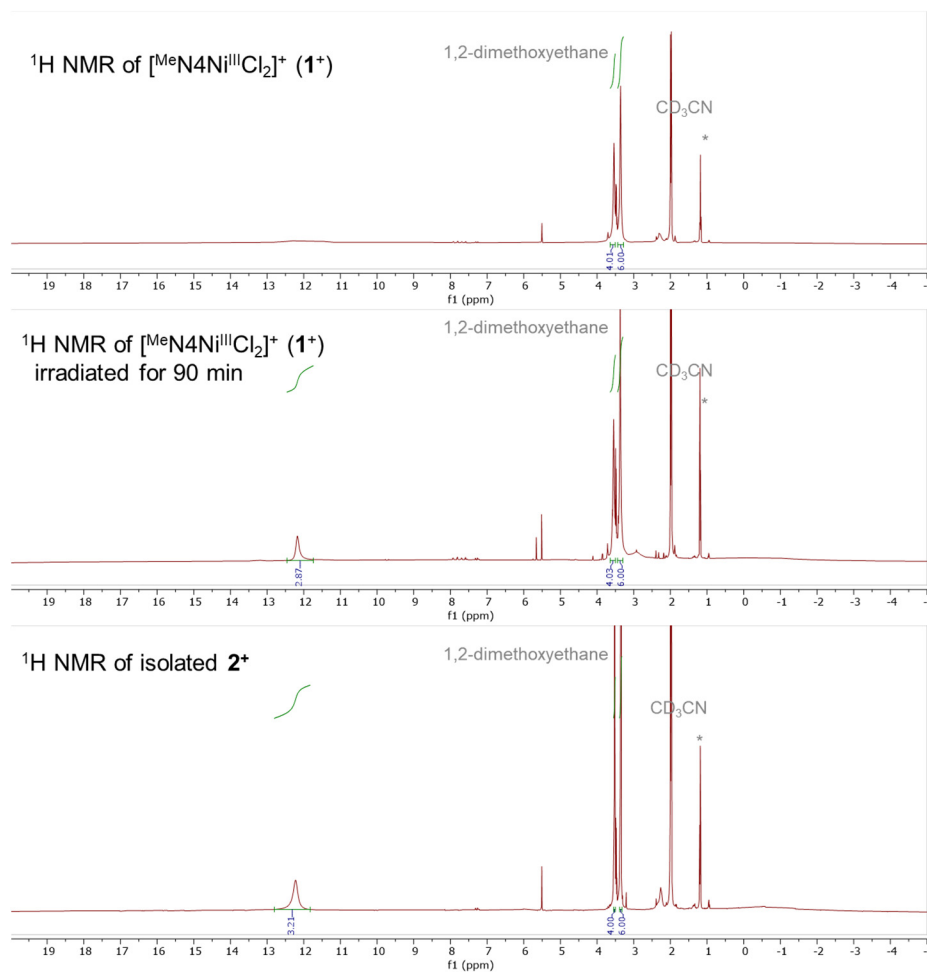


Figure S12. Enlarged, stacked paramagnetic ^1H NMR spectra of 1^+ before and after photolysis, and independently synthesized 2^+ , for quantification of the photoreduction product. The compound 1^+ is NMR inactive. All spectra were recorded at 500 MHz and referenced to the CD_3CN solvent peak. (* = Et_2O)

7. UV-vis absorption spectra of 2^+ after addition of PhICl_2

A 2 mM 2^+ solution in CH_3CN (2 mL) was irradiated with blue LED for 10min to generate 2^+ by photoreduction. The absorption spectrum of 2^+ was collected (black line). To this solution, CH_3CN solution of 1 equiv PhICl_2 (0.1 mL) was added. An increase of absorption band at 563 nm was observed over time. At this low concentration (for UV-visible absorbance detection purpose), reaction between PhICl_2 and 2^+ was slow, requiring over 20 min to achieve significant conversion.

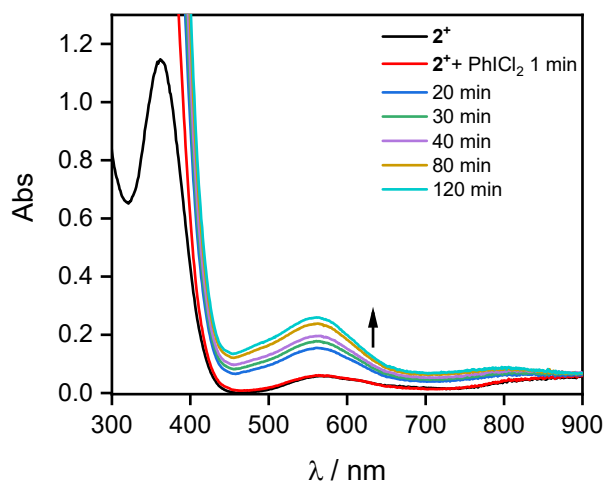


Figure S13. UV-vis absorption spectrum for 2^+ after addition of PhICl_2 . Increase of the band at 530 nm indicates regeneration of 1^+ .

9. Quantum yield measurement for the photolysis of 1^+

The photolysis reaction was performed with one Kessil lamp model PR160 blue LED ($\lambda_{\max} = 456$ nm, max 50 W). Potassium ferrioxalate was prepared following the published procedure as a standard actinometer ($\Phi_s = 1.12$ at 458 nm (0.01 M)).⁶ Actinometry was conducted following the well-known procedure, generating $[\text{Fe}(\text{phen})_3]^{2+}$ with addition of the buffer solution of 1,10-phenanthroline (phen) after irradiation.⁶⁻⁸

The quantum yield of the photolysis reaction (Φ_{1^+}) was determined according to equation (1), following a literature procedure:⁹

$$\Phi_{1^+} = \Phi_s \times (\Delta C_{1^+} \times V_{1^+}) / (\Delta C_s \times V_s) \quad \text{Equation (1)}$$

Where Φ_s is the quantum yield of the standard, ΔC_s and ΔC_{1^+} are the concentration differences before and after irradiation, and V_s and V_{1^+} are volumes (corresponding to the dilution factor) of the standard and 1^+ , respectively. ΔC_s and ΔC_{1^+} could be calculated based on the absorbance differences (ΔA_s and ΔA_{1^+}) using ϵ_s and ϵ_{1^+} . The solution of the standard (in 0.05 M H_2SO_4) and 1^+ (in CH_3CN) were sufficiently concentrated ($[\text{standard}] = 0.01$ M, $[1^+] = 1.3$ mM) to assume 100% absorption of the incident light. The standard and sample solution were irradiated for the same time (20 s). The extinction coefficient of $\epsilon_s = 11100 \text{ M}^{-1}\text{cm}^{-1}$ at 510 nm (reported value in the literature⁶) and $\epsilon_{1^+} = 211 \text{ M}^{-1}\text{cm}^{-1}$ at 563 nm were used.

10. Solid-state photolysis

Photolysis of [1]BF₄ as a suspension in THF

Compound [1]BF₄ (4 mg) was transferred into the glass capillary with THF as transferring medium (compound [1]BF₄ and [2]BF₄ are not soluble in THF). The sample was irradiated with 456 nm blue LED for 1 h. Color change from dark purple to light blue was observed, indicating a solid-state photoreduction reaction.

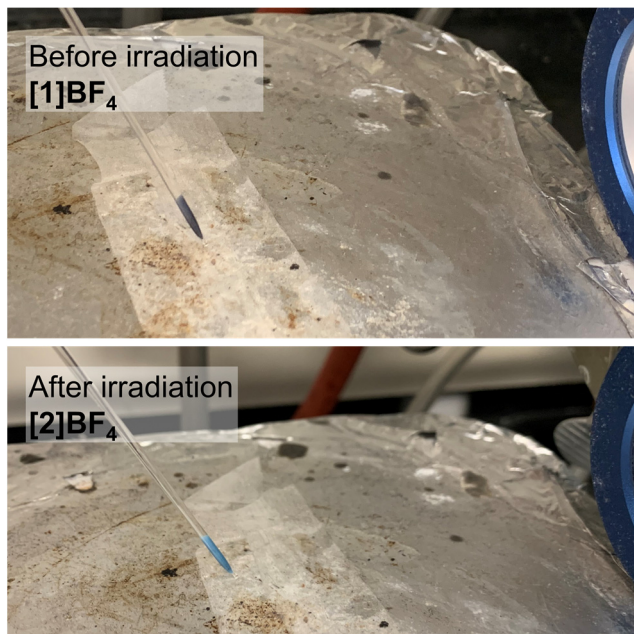


Figure S14. Color change of solid sample of [1]BF₄ after irradiation with 456 nm blue LED for 1 h, demonstrating solid-state photoreduction reaction.

Photolysis of [1]BF₄ as a dry solid

Compound [1]BF₄ (5 mg, 0.01 mmol) was transferred into the 20 mL vial inside of the glove box and then brought out of the glove box. (Note that for this reaction, a vial used instead of a capillary, due to the static of 1⁺ originating from the gloves, which prevents efficient transporting of solid samples.) The sample was irradiated with blue LED for 10 h. Color change from a dark purple to light blue was observed, indicating the formation of [^{Me}N₄Ni^{II}Cl]⁺ species (Figure S15). The solid sample was brought into the glovebox, dissolved in CD₃CN (0.4 mL), and transferred into the NMR tube. Into the NMR tube, 0.1 mL of stock solution of 1,2-dimethoxyethane in CD₃CN (0.01 mmol, 1 equiv) was added (stock solution prepared: 11 μL of 1,2 dimethoxyethane in 1 mL of CD₃CN) as an internal standard to obtain ¹H NMR spectrum. After shaking the sample, ¹H NMR

spectrum was collected. The obtained ^1H NMR spectrum is identical to that of independently synthesized 2^+ , confirming that solid-state photolysis can be carried out in the absence of a trap, as shown in Figure S16. As a separate sample, independently synthesized 2^+ (5.6 mg, 0.01 mmol) was dissolved in 0.4 mL of CD_3CN and 0.1 mL of stock solution of 1,2-dimethoxyethane in CD_3CN (stock solution prepared: 11 μL of 1,2 dimethoxyethane in 1 mL of CD_3CN) as a standard. After shaking the sample, ^1H NMR spectrum was collected. As the compound exhibits paramagnetic shifts, well-resolved peaks (12.2 ppm) of irradiated sample and 2^+ were integrated relative to the peaks of 1,2-dimethoxyethane. The amount of 2^+ generated was calculated to be 67% (Figure S17 and S18).

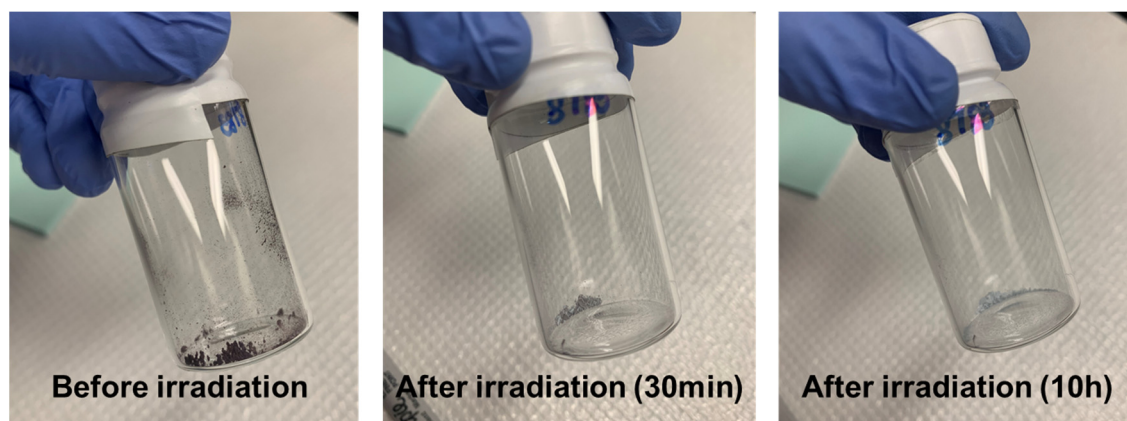


Figure S15. Color change of solid sample of $[\mathbf{1}]\text{BF}_4$ after irradiation with blue LED for 10 h, demonstrating solid-state photoreduction reaction.

Halide elemental analysis

To additionally support the yield of solid-state photolysis reaction, we performed halide elemental analysis of the irradiated sample. Compound $[\mathbf{1}]\text{BF}_4$ (10 mg, 0.02 mmol) was transferred into the 20 mL vial inside of the glove box and then brought out of the glove box. After irradiation with blue LED for 10 h, the vial was brought into the glovebox. The elemental analysis samples of $[\mathbf{1}]\text{BF}_4$ (non-irradiated sample) and irradiated compound were prepared inside the glovebox. The halide elemental analysis was conducted, and Cl% of the non-irradiated $[\mathbf{1}]\text{BF}_4$ and the irradiated sample were compared.

Elemental analysis for $[1]BF_4$ (non-irradiated sample): found Cl, 14.50%; calculated $C_{16}H_{20}BCl_2F_4N_4Ni$, 14.63%

Elemental analysis for $[^{Me}N_4Ni^{II}Cl]BF_4$ (irradiated sample): found Cl, 10.47%; calculated for 100% conversion to $C_{16}H_{20}BCl_2F_4N_4Ni$, 7.89%.

A decrease of Cl% value from 14.50% to 10.47% was observed after photolysis. Based on the calculation, 36% of $[1]BF_4$ + 64% of $[^{Me}N_4Ni^{II}Cl]BF_4$ gave Cl 10.43% ($0.36 \cdot C_{16}H_{20}BCl_2F_4N_4Ni$ + $0.64 \cdot C_{16}H_{20}BClF_4N_4Ni$), thus confirming the yield of the solid-state photolysis is 64%. This 64% yield matches very well the 67% yield obtained from 1H NMR integration.

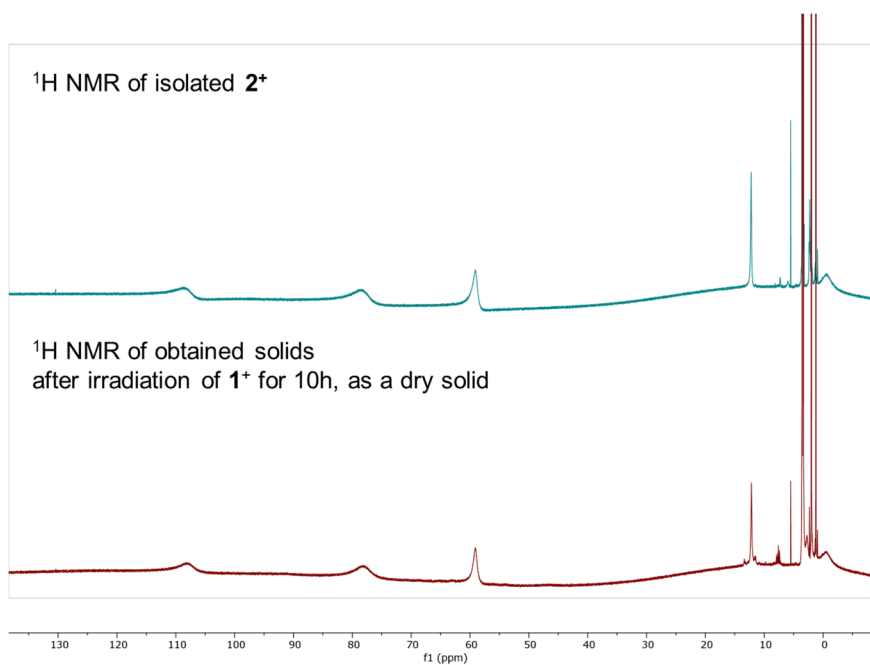


Figure S16. Comparison of 1H NMR spectra of 2^+ and the irradiated solid sample, confirming solid-state photolysis.

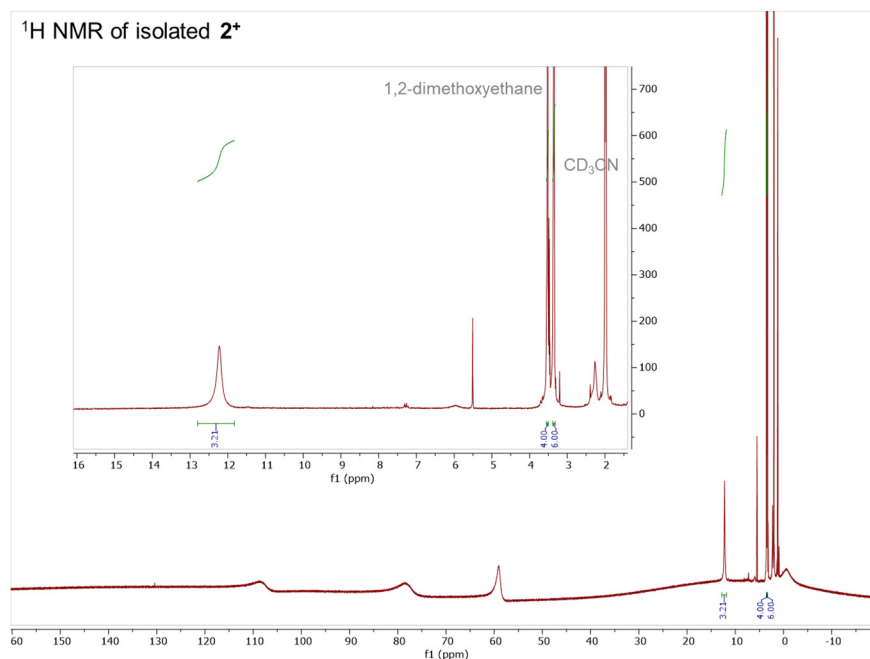


Figure S17. Paramagnetic ¹H NMR spectrum of **2**⁺ (0.01 mmol) with the 1,2-dimethoxyethane standard.

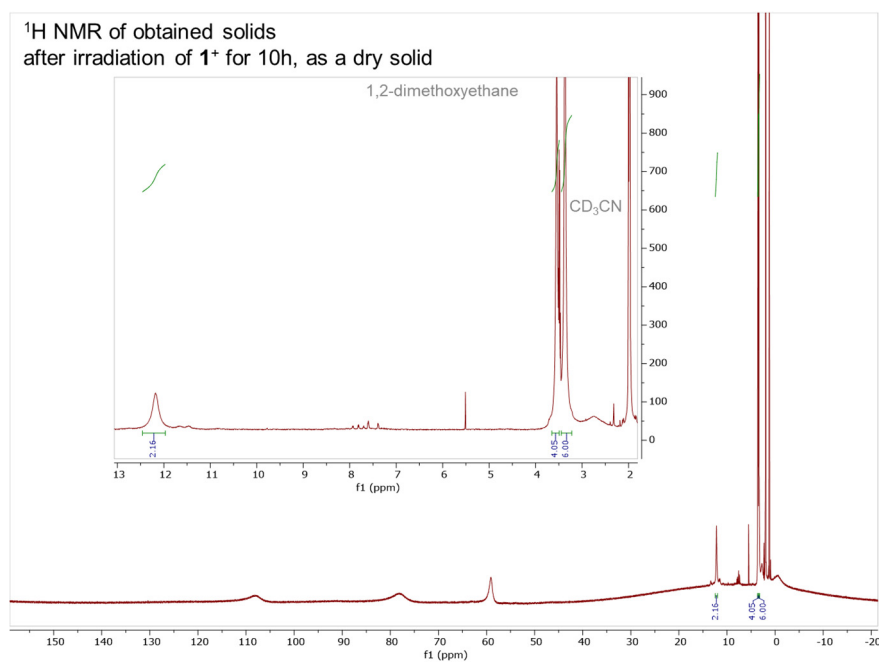


Figure S18. Paramagnetic ¹H NMR spectrum of the irradiated solid sample (0.01 mmol of **1**⁺ was irradiated) with the 1,2-dimethoxyethane standard.

Cl₂ gas detection experiment: DPD colorimetric method

To support Cl₂ gas formation through solid-state photolysis, we performed DPD colorimetric chlorine test. Compound [1]BF₄ (5 mg, 0.01 mmol) was transferred into the 4 mL vial inside of the glove box, and sealed with a septum and electrical tape, then brought out of the glove box. After 10 h irradiation with blue LED, headspace gas of the reaction was transferred to the vial containing *N,N*-diethyl-1,4-phenylenediamine (DPD) sulfate (2.6 mg) in 2 mL of DI water (5 mM). Then the reaction mixture was shaken vigorously. The clear solution color was changed into pink color, indicating radical cation DPD^{•+}, as shown in Figure S19. The formation of DPD^{•+} was monitored by UV-vis absorption spectroscopy. The obtained absorption spectrum matched the known spectrum of the DPD-Wurster compound, with λ_{\max} values of 511 nm and 552 nm.

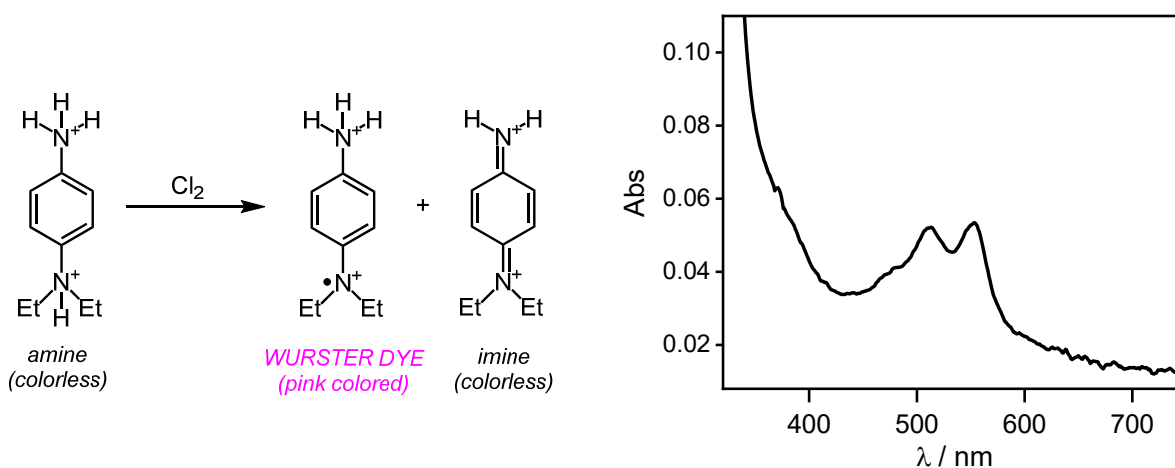


Figure S19. DPD-Chlorine reaction (left) and absorption spectrum of the reaction mixture (right), showing formation of DPD^{•+}.

11. PBN spin trapping EPR study

4 mg of solid compound [1]BF₄ was transferred into the capillary (as shown in Figure S14) using THF as a transporting medium ([1]BF₄ is not soluble in THF) with 14.6 mg (10 equiv) of *N*-tert-butyl- α -phenylnitron (PBN). After irradiation of the sample for 2 h with blue LED, the EPR spectrum was recorded at room temperature. The parameters used for the simulation are similar to those reported previously for the PBN-THF adduct.^{10,11}

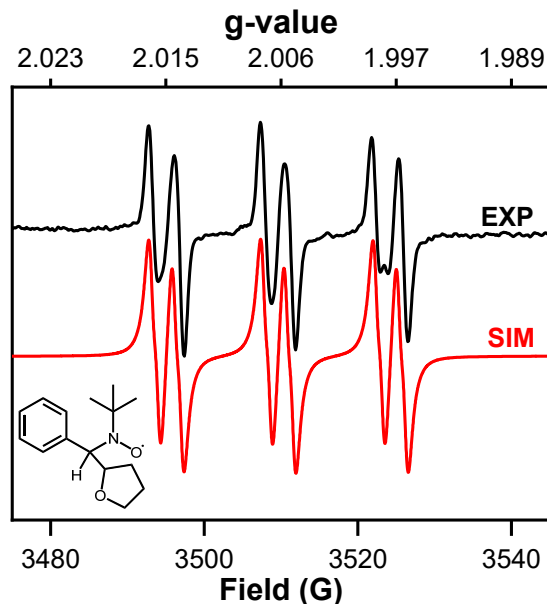


Figure S20. EPR spectrum of irradiated solid [1]BF₄ in the presence of PBN. Parameters used for simulation: $g = 2.0061$, $A_N = 14.6$ G, $A_H = 3.0$ G, $A_C(\text{THF}) = 3.0$ G, $A_H(\text{THF}) = 0.90$ G, linewidth 1.15 G.

12. X-ray structure characterization

General information.

Single crystals of [1]PF₆ were grown by vapor diffusion of pentane into a concentrated solution of CH₂Cl₂ at -35 °C. Suitable crystals of appropriate dimensions were mounted on Mitegen loops in random orientations. Preliminary examination and data collection were performed using a Bruker Kappa Apex-II Charge Coupled Device (CCD) Detector system single crystal X-Ray diffractometer equipped with an Oxford Cryostream LT device. Data were collected using graphite monochromated Mo K α radiation ($\lambda = 0.71073 \text{ \AA}$) from a fine focus sealed tube X-Ray source. Preliminary unit cell constants were determined with a set of 36 narrow frame scans. Typical data sets consist of combinations of ω and ϕ scan frames with typical scan width of 0.5° and counting time of 15-30 seconds/frame at a crystal to detector distance of 3.0 to 3.5 cm. The collected frames were integrated using an orientation matrix determined from the narrow frame scans. Apex II and SAINT software packages (Bruker Analytical X-Ray, Madison, WI, 2008) were used for data collection and data integration. Final cell constants were determined by global refinement of reflections from the complete data set. Data were corrected for systematic errors using SADABS (Bruker Analytical X-Ray, Madison, WI, 2008) based on the Laue symmetry using equivalent reflections. Structure solutions and refinement were carried out using the SHELXTL- PLUS software package¹². The structures were refined with full matrix least-squares refinement by minimizing $\sum w(F_o^2 - F_c^2)^2$. All non-hydrogen atoms were refined anisotropically to convergence.

Single crystals of [2]PF₆ were grown by vapor diffusion of pentane into concentrated solution of CH₃Cl and MeOH at -35 °C. Crystals were mounted on a Bruker D8 Venture kappa diffractometer equipped with a Photon II CPAD detector. An I μ s microfocus Mo source ($\lambda = 0.71073 \text{ \AA}$) coupled with a multi-layer mirror monochromator provided the incident beam. The sample was mounted on a nylon loop with the minimal amount of Paratone-N oil. Data was collected as a series of ϕ and/or ω scans. Data was collected at 100 K using a cold stream of N₂(g). The collection, cell refinement, and integration of intensity data was carried out with the APEXIII software.¹³ A multiscan absorption correction was performed with SADABS.¹⁴ The structure was phased with intrinsic methods using SHELXT and refined with the full-matrix least-squares program SHELXL.¹² Hydrogen atoms were placed in calculated positions using the standard riding model and refined isotropically; all non-hydrogen atoms were refined anisotropically.

Computer programs: *SAINT* V8.38A (2016), *SHELXT* (Sheldrick, 2015), *XL* (Sheldrick, 2008), *Olex2* (Dolomanov *et al.*, 2009).

CCDC numbers 2076279 and 2076280 contain the supplementary crystallographic data for this paper. These data are provided free of charge by the Cambridge Crystallographic Data Centre. Crystallographic details are summarized in Tables S1 and S3.

Table S1. Crystal data and structure refinement for [1]PF₆

Crystal data	
Chemical formula	C ₁₆ H ₂₀ Cl ₂ N ₄ Ni·F ₆ P
<i>M_r</i>	542.94
Crystal system, space group	Monoclinic, <i>P2₁/c</i>
Temperature (K)	100
<i>a</i> , <i>b</i> , <i>c</i> (Å)	12.9385 (3), 12.1873 (3), 12.9860 (3)
<i>β</i> (°)	101.5138 (15)
<i>V</i> (Å ³)	2006.50 (8)
<i>Z</i>	4
Radiation type	Mo <i>K</i> _α
<i>μ</i> (mm ⁻¹)	1.38
Crystal size (mm)	0.30 × 0.27 × 0.10
Data collection	
Diffractometer	Bruker <i>APEX-II</i> CCD
Absorption correction	Multi-scan <i>SADABS</i> v2012/1
<i>T_{min}</i> , <i>T_{max}</i>	0.674, 0.862
No. of measured, independent and observed [<i>I</i> > 2 <i>s</i> (<i>I</i>)] reflections	24160, 4618, 3449
<i>R_{int}</i>	0.066
(<i>sin</i> <i>q/l</i>) _{max} (Å ⁻¹)	0.651
Refinement	
<i>R</i> [<i>F</i> ² > 2 <i>s</i> (<i>F</i> ²)], <i>wR</i> (<i>F</i> ²), <i>S</i>	0.045, 0.113, 1.02
No. of reflections	4618
No. of parameters	399
No. of restraints	590
H-atom treatment	H-atom parameters constrained
<i>D</i> _{ρmax} , <i>D</i> _{ρmin} (e Å ⁻³)	0.70, -0.61

Computer programs: Bruker *APEX2*, Bruker *SAINT*, *SHELXT2013* (Sheldrick, 2008), *SHELXL2014* (Sheldrick, 2014), Bruker *SHELXTL*.

Table S2. Bond length (Å) and angles (°) for [1]PF₆

Ni1—N2	1.869 (9)	N2—C12	1.327 (11)
Ni1—N1	1.900 (3)	C8—C9	1.374 (12)
Ni1—N2'	1.916 (6)	C9—C10	1.355 (15)
Ni1—N4	2.159 (3)	C9—H9	0.9500
Ni1—N3	2.159 (3)	C10—C11	1.383 (15)
Ni1—C12	2.1885 (9)	C10—H10	0.9500
Ni1—C11	2.2138 (9)	C11—C12	1.385 (11)
N1—C5	1.333 (4)	C11—H11	0.9500
N1—C1	1.340 (4)	C12—C13	1.486 (14)
N3—C14	1.463 (5)	N2'—C12'	1.333 (8)
N3—C15	1.468 (5)	N2'—C8'	1.338 (8)
N3—C13'	1.473 (8)	C8'—C9'	1.402 (10)
N3—C13	1.562 (12)	C9'—C10'	1.354 (11)
N4—C7	1.307 (10)	C9'—H9'	0.9500
N4—C16'	1.427 (8)	C10'—C11'	1.402 (11)
N4—C6	1.471 (5)	C10'—H10'	0.9500
N4—C7'	1.604 (8)	C11'—C12'	1.375 (8)
N4—C16	1.686 (13)	C11'—H11'	0.9500
C1—C2	1.377 (5)	C12'—C13'	1.509 (9)
C1—C14	1.490 (5)	C13—H13A	0.9900
C2—C3	1.371 (6)	C13—H13B	0.9900
C2—H2	0.9500	C16—H16A	0.9800
C3—C4	1.379 (5)	C16—H16B	0.9800
C3—H3	0.9500	C16—H16C	0.9800
C4—C5	1.381 (5)	C13'—H13C	0.9900
C4—H4	0.9500	C13'—H13D	0.9900
C5—C6	1.505 (5)	C16'—H16D	0.9800
C6—H6A	0.9900	C16'—H16E	0.9800
C6—H6B	0.9900	C16'—H16F	0.9800
C14—H14A	0.9900	P1—F5'	1.545 (6)
C14—H14B	0.9900	P1—F3	1.568 (3)
C15—H15A	0.9800	P1—F5	1.572 (3)
C15—H15B	0.9800	P1—F4	1.578 (3)
C15—H15C	0.9800	P1—F3'	1.585 (6)
C7—C8	1.484 (14)	P1—F2'	1.587 (6)
C7—H7A	0.9900	P1—F4'	1.589 (6)
C7—H7B	0.9900	P1—F1'	1.594 (6)
C7'—C8'	1.515 (9)	P1—F1	1.604 (3)
C7'—H7'1	0.9900	P1—F2	1.604 (3)
C7'—H7'2	0.9900	P1—F6	1.610 (3)
N2—C8	1.323 (11)	P1—F6'	1.629 (6)
<hr/>			
N2—Ni1—N1	86.1 (5)	C8—N2—Ni1	119.2 (8)

N1—Ni1—N2'	91.1 (4)	C12—N2—Ni1	116.7 (8)
N2—Ni1—N4	76.1 (3)	N2—C8—C9	118.7 (11)
N1—Ni1—N4	81.43 (11)	N2—C8—C7	117.2 (9)
N2'—Ni1—N4	87.0 (2)	C9—C8—C7	123.3 (9)
N2—Ni1—N3	88.1 (4)	C10—C9—C8	118.8 (11)
N1—Ni1—N3	82.97 (12)	C10—C9—H9	120.6
N2'—Ni1—N3	78.5 (2)	C8—C9—H9	120.6
N4—Ni1—N3	158.40 (13)	C9—C10—C11	122.0 (10)
N2—Ni1—C12	171.6 (4)	C9—C10—H10	119.0
N1—Ni1—C12	88.85 (8)	C11—C10—H10	119.0
N2'—Ni1—C12	176.4 (2)	C10—C11—C12	117.0 (10)
N4—Ni1—C12	96.56 (11)	C10—C11—H11	121.5
N3—Ni1—C12	97.97 (8)	C12—C11—H11	121.5
N2—Ni1—C11	92.2 (5)	N2—C12—C11	119.2 (10)
N1—Ni1—C11	178.28 (8)	N2—C12—C13	117.6 (9)
N2'—Ni1—C11	87.2 (4)	C11—C12—C13	123.0 (10)
N4—Ni1—C11	98.26 (9)	C12'—N2'—C8'	121.8 (6)
N3—Ni1—C11	96.88 (9)	C12'—N2'—Ni1	119.4 (5)
C12—Ni1—C11	92.87 (3)	C8'—N2'—Ni1	118.8 (5)
C5—N1—C1	121.9 (3)	N2'—C8'—C9'	120.4 (7)
C5—N1—Ni1	119.0 (2)	N2'—C8'—C7'	116.2 (6)
C1—N1—Ni1	119.0 (2)	C9'—C8'—C7'	123.3 (6)
C14—N3—C15	108.7 (3)	C10'—C9'—C8'	117.9 (7)
C14—N3—C13'	121.3 (5)	C10'—C9'—H9'	121.1
C15—N3—C13'	100.2 (4)	C8'—C9'—H9'	121.1
C14—N3—C13	96.8 (7)	C9'—C10'—C11'	121.3 (6)
C15—N3—C13	126.5 (6)	C9'—C10'—H10'	119.4
C14—N3—Ni1	106.9 (2)	C11'—C10'—H10'	119.4
C15—N3—Ni1	115.3 (3)	C12'—C11'—C10'	118.0 (7)
C13'—N3—Ni1	104.7 (3)	C12'—C11'—H11'	121.0
C13—N3—Ni1	100.0 (4)	C10'—C11'—H11'	121.0
C7—N4—C6	123.0 (6)	N2'—C12'—C11'	120.5 (6)
C16'—N4—C6	118.6 (4)	N2'—C12'—C13'	114.1 (6)
C16'—N4—C7'	107.1 (5)	C11'—C12'—C13'	125.2 (6)
C6—N4—C7'	106.4 (4)	C12—C13—N3	116.1 (8)
C7—N4—C16	111.1 (7)	C12—C13—H13A	108.3
C6—N4—C16	96.3 (6)	N3—C13—H13A	108.3
C7—N4—Ni1	113.4 (5)	C12—C13—H13B	108.3
C16'—N4—Ni1	116.2 (4)	N3—C13—H13B	108.3
C6—N4—Ni1	104.8 (2)	H13A—C13—H13B	107.4
C7'—N4—Ni1	102.1 (3)	N4—C16—H16A	109.5
C16—N4—Ni1	105.9 (4)	N4—C16—H16B	109.5
N1—C1—C2	119.8 (3)	H16A—C16—H16B	109.5
N1—C1—C14	116.2 (3)	N4—C16—H16C	109.5
C2—C1—C14	124.0 (3)	H16A—C16—H16C	109.5

C3—C2—C1	119.1 (3)	H16B—C16—H16C	109.5
C3—C2—H2	120.5	N3—C13'—C12'	106.6 (5)
C1—C2—H2	120.5	N3—C13'—H13C	110.4
C2—C3—C4	120.5 (3)	C12'—C13'—H13C	110.4
C2—C3—H3	119.8	N3—C13'—H13D	110.4
C4—C3—H3	119.8	C12'—C13'—H13D	110.4
C3—C4—C5	118.3 (3)	H13C—C13'—H13D	108.6
C3—C4—H4	120.8	N4—C16'—H16D	109.5
C5—C4—H4	120.8	N4—C16'—H16E	109.5
N1—C5—C4	120.3 (3)	H16D—C16'—H16E	109.5
N1—C5—C6	115.0 (3)	N4—C16'—H16F	109.5
C4—C5—C6	124.5 (3)	H16D—C16'—H16F	109.5
N4—C6—C5	110.9 (3)	H16E—C16'—H16F	109.5
N4—C6—H6A	109.5	F3—P1—F5	93.5 (2)
C5—C6—H6A	109.5	F3—P1—F4	92.7 (2)
N4—C6—H6B	109.5	F5—P1—F4	91.5 (2)
C5—C6—H6B	109.5	F5'—P1—F3'	92.3 (6)
H6A—C6—H6B	108.1	F5'—P1—F2'	92.8 (6)
N3—C14—C1	114.6 (3)	F3'—P1—F2'	90.9 (5)
N3—C14—H14A	108.6	F5'—P1—F4'	93.5 (6)
C1—C14—H14A	108.6	F3'—P1—F4'	88.8 (6)
N3—C14—H14B	108.6	F2'—P1—F4'	173.7 (6)
C1—C14—H14B	108.6	F5'—P1—F1'	92.9 (6)
H14A—C14—H14B	107.6	F3'—P1—F1'	174.4 (6)
N3—C15—H15A	109.5	F2'—P1—F1'	90.8 (5)
N3—C15—H15B	109.5	F4'—P1—F1'	88.8 (6)
H15A—C15—H15B	109.5	F3—P1—F1	176.8 (2)
N3—C15—H15C	109.5	F5—P1—F1	88.93 (18)
H15A—C15—H15C	109.5	F4—P1—F1	89.30 (19)
H15B—C15—H15C	109.5	F3—P1—F2	89.10 (19)
N4—C7—C8	105.1 (7)	F5—P1—F2	90.49 (19)
N4—C7—H7A	110.7	F4—P1—F2	177.2 (2)
C8—C7—H7A	110.7	F1—P1—F2	88.78 (18)
N4—C7—H7B	110.7	F3—P1—F6	89.2 (2)
C8—C7—H7B	110.7	F5—P1—F6	177.1 (2)
H7A—C7—H7B	108.8	F4—P1—F6	89.23 (19)
C8'—C7'—N4	115.4 (5)	F1—P1—F6	88.30 (18)
C8'—C7'—H7'1	108.4	F2—P1—F6	88.68 (18)
N4—C7'—H7'1	108.4	F5'—P1—F6'	179.4 (6)
C8'—C7'—H7'2	108.4	F3'—P1—F6'	88.3 (5)
N4—C7'—H7'2	108.4	F2'—P1—F6'	87.2 (5)
H7'1—C7'—H7'2	107.5	F4'—P1—F6'	86.5 (5)
C8—N2—C12	124.1 (9)	F1'—P1—F6'	86.5 (5)

Table S3. Crystal data and structure refinement for [2]PF₆

Crystal data	
Chemical formula	C ₁₇ H ₂₄ ClN ₄ NiO·CHCl ₃ ·F ₆ P
M_r	658.90
Crystal system, space group	Orthorhombic, <i>Pna</i> 2 ₁
Temperature (K)	100
a, b, c (Å)	19.4628 (6), 13.3212 (4), 9.6192 (3)
V (Å ³)	2493.95 (13)
Z	4
Radiation type	Mo <i>K</i> α
μ (mm ⁻¹)	1.34
Crystal size (mm)	0.68 × 0.16 × 0.04
Data collection	
Diffractometer	Bruker <i>APEX-II</i> CCD
Absorption correction	Multi-scan <i>SADABS2016/2</i> (Bruker,2016/2) was used for absorption correction. $wR2(\text{int})$ was 0.1430 before and 0.0567 after correction. The Ratio of minimum to maximum transmission is 0.8015. The 1/2 correction factor is Not present.
$T_{\text{min}}, T_{\text{max}}$	0.598, 0.746
No. of measured, independent and observed [$I > 2s(I)$] reflections	47334, 5725, 5629
R_{int}	0.042
$(\sin \theta/\lambda)_{\text{max}}$ (Å ⁻¹)	0.649
Refinement	
$R[F^2 > 2s(F^2)], wR(F^2), S$	0.032, 0.104, 0.97
No. of reflections	5725
No. of parameters	359
No. of restraints	140
H-atom treatment	H atoms treated by a mixture of independent and constrained refinement
$D\rho_{\text{max}}, D\rho_{\text{min}}$ (e Å ⁻³)	0.70, -1.29
Absolute structure	Flack x determined using 2592 quotients $[(I^+)-(I^-)]/[(I^+)+(I^-)]$ (Parsons, Flack and Wagner, <i>Acta Cryst.</i> B69 (2013) 249-259).
Absolute structure parameter	0.015 (4)

Table S4. Bond length (Å) and angles (°) for [2]PF₆

Ni1—C11	2.3611 (8)	N3—C16	1.474 (5)
Ni1—N1	2.009 (3)	C2—H2	0.9500
Ni1—N4	2.189 (3)	C2—C3	1.392 (6)
Ni1—O1	2.065 (3)	C13—H13A	0.9900
Ni1—N2	2.034 (3)	C13—H13B	0.9900
Ni1—N3	2.197 (3)	C8—C9	1.395 (5)
Cl2—C18	1.756 (4)	C8—C7	1.508 (5)
Cl4—C18	1.754 (4)	C9—H9	0.9500
P1—F1	1.576 (3)	C9—C10	1.389 (6)
P1—F3	1.585 (3)	C11—H11	0.9500
P1—F6	1.483 (7)	C11—C10	1.390 (6)
P1—F2	1.600 (6)	C7—H7A	0.9900
P1—F5	1.668 (7)	C7—H7B	0.9900
P1—F4	1.588 (6)	C3—H3	0.9500
P1—F6A	1.606 (6)	C3—C4	1.387 (6)
P1—F2A	1.667 (5)	C5—C6	1.521 (6)
P1—F5A	1.553 (6)	C5—C4	1.387 (5)
P1—F4A	1.527 (5)	C10—H10	0.9500
Cl3—C18	1.734 (4)	C6—H6A	0.9900
N1—C1	1.334 (5)	C6—H6B	0.9900
N1—C5	1.333 (5)	C15—H15A	0.9800
N4—C13	1.496 (4)	C15—H15B	0.9800
N4—C15	1.473 (5)	C15—H15C	0.9800
N4—C14	1.483 (4)	C14—H14A	0.9900
O1—H1	0.881 (13)	C14—H14B	0.9900
O1—C17	1.434 (4)	C4—H4	0.9500
N2—C12	1.342 (4)	C18—H18	1.0000
N2—C8	1.333 (5)	C16—H16A	0.9800
C1—C2	1.393 (5)	C16—H16B	0.9800
C1—C14	1.506 (5)	C16—H16C	0.9800
C12—C13	1.505 (5)	C17—H17A	0.9800
C12—C11	1.388 (5)	C17—H17B	0.9800
N3—C7	1.496 (5)	C17—H17C	0.9800
N3—C6	1.483 (5)		
<hr/>			
N1—Ni1—C11	96.83 (8)	C3—C2—C1	118.4 (4)
N1—Ni1—N4	80.81 (12)	C3—C2—H2	120.8
N1—Ni1—O1	176.70 (12)	N4—C13—C12	111.7 (3)
N1—Ni1—N2	83.58 (11)	N4—C13—H13A	109.3
N1—Ni1—N3	80.93 (13)	N4—C13—H13B	109.3
N4—Ni1—C11	99.45 (8)	C12—C13—H13A	109.3
N4—Ni1—N3	154.45 (12)	C12—C13—H13B	109.3
O1—Ni1—C11	85.82 (7)	H13A—C13—H13B	107.9

O1—Ni1—N4	96.84 (12)	N2—C8—C9	121.2 (3)
O1—Ni1—N3	100.57 (13)	N2—C8—C7	114.3 (3)
N2—Ni1—C11	179.58 (9)	C9—C8—C7	124.5 (3)
N2—Ni1—N4	80.48 (12)	C8—C9—H9	120.8
N2—Ni1—O1	93.77 (11)	C10—C9—C8	118.4 (3)
N2—Ni1—N3	79.85 (12)	C10—C9—H9	120.8
N3—Ni1—C11	100.33 (9)	C12—C11—H11	120.5
F1—P1—F3	178.3 (2)	C12—C11—C10	118.9 (3)
F1—P1—F2	97.2 (3)	C10—C11—H11	120.5
F1—P1—F5	89.6 (3)	N3—C7—C8	111.3 (3)
F1—P1—F4	84.3 (3)	N3—C7—H7A	109.4
F1—P1—F6A	97.1 (4)	N3—C7—H7B	109.4
F1—P1—F2A	85.7 (2)	C8—C7—H7A	109.4
F3—P1—F2	81.2 (3)	C8—C7—H7B	109.4
F3—P1—F5	91.1 (3)	H7A—C7—H7B	108.0
F3—P1—F4	97.3 (3)	C2—C3—H3	119.9
F3—P1—F6A	83.6 (4)	C4—C3—C2	120.2 (3)
F3—P1—F2A	92.8 (3)	C4—C3—H3	119.9
F6—P1—F1	89.3 (4)	N1—C5—C6	114.1 (3)
F6—P1—F3	89.9 (4)	N1—C5—C4	120.9 (4)
F6—P1—F2	92.1 (5)	C4—C5—C6	125.0 (4)
F6—P1—F5	178.0 (6)	C9—C10—C11	119.6 (3)
F6—P1—F4	94.6 (6)	C9—C10—H10	120.2
F2—P1—F5	86.4 (5)	C11—C10—H10	120.2
F4—P1—F2	173.1 (5)	N3—C6—C5	111.7 (3)
F4—P1—F5	86.9 (5)	N3—C6—H6A	109.3
F6A—P1—F2A	85.5 (4)	N3—C6—H6B	109.3
F5A—P1—F1	85.3 (3)	C5—C6—H6A	109.3
F5A—P1—F3	93.8 (3)	C5—C6—H6B	109.3
F5A—P1—F6A	173.4 (5)	H6A—C6—H6B	107.9
F5A—P1—F2A	88.6 (4)	N4—C15—H15A	109.5
F4A—P1—F1	94.1 (3)	N4—C15—H15B	109.5
F4A—P1—F3	87.5 (3)	N4—C15—H15C	109.5
F4A—P1—F6A	90.4 (4)	H15A—C15—H15B	109.5
F4A—P1—F2A	175.9 (5)	H15A—C15—H15C	109.5
F4A—P1—F5A	95.5 (4)	H15B—C15—H15C	109.5
C1—N1—Ni1	117.5 (2)	N4—C14—C1	111.8 (3)
C5—N1—Ni1	117.6 (2)	N4—C14—H14A	109.2
C5—N1—C1	122.0 (3)	N4—C14—H14B	109.2
C13—N4—Ni1	106.6 (2)	C1—C14—H14A	109.2
C15—N4—Ni1	114.5 (2)	C1—C14—H14B	109.2
C15—N4—C13	109.6 (3)	H14A—C14—H14B	107.9
C15—N4—C14	109.6 (3)	C3—C4—H4	120.9
C14—N4—Ni1	105.6 (2)	C5—C4—C3	118.2 (4)
C14—N4—C13	110.9 (3)	C5—C4—H4	120.9

Ni1—O1—H1	125.1 (19)	Cl2—C18—H18	107.5
C17—O1—Ni1	127.6 (2)	Cl4—C18—Cl2	111.3 (2)
C17—O1—H1	103.8 (18)	Cl4—C18—H18	107.5
C12—N2—Ni1	117.2 (2)	Cl3—C18—Cl2	112.8 (3)
C8—N2—Ni1	118.1 (2)	Cl3—C18—Cl4	110.0 (2)
C8—N2—C12	120.9 (3)	Cl3—C18—H18	107.5
N1—C1—C2	120.2 (4)	N3—C16—H16A	109.5
N1—C1—C14	114.6 (3)	N3—C16—H16B	109.5
C2—C1—C14	125.2 (3)	N3—C16—H16C	109.5
N2—C12—C13	114.3 (3)	H16A—C16—H16B	109.5
N2—C12—C11	120.9 (3)	H16A—C16—H16C	109.5
C11—C12—C13	124.8 (3)	H16B—C16—H16C	109.5
C7—N3—Ni1	106.8 (2)	O1—C17—H17A	109.5
C6—N3—Ni1	105.6 (2)	O1—C17—H17B	109.5
C6—N3—C7	110.7 (3)	O1—C17—H17C	109.5
C16—N3—Ni1	114.2 (2)	H17A—C17—H17B	109.5
C16—N3—C7	109.7 (3)	H17A—C17—H17C	109.5
C16—N3—C6	109.8 (3)	H17B—C17—H17C	109.5
C1—C2—H2	120.8		

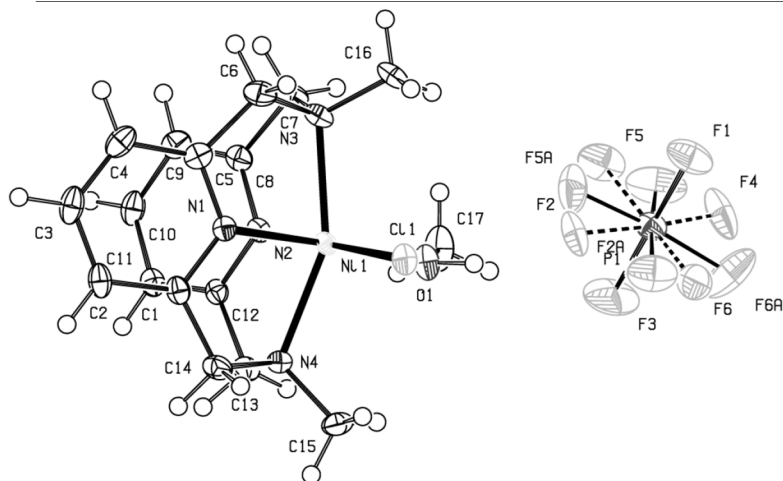


Figure S22. Projection view of $[\text{Me}_4\text{N}_4\text{Ni}^{\text{II}}\text{Cl}(\text{MeOH})]\text{PF}_6$ ($[\mathbf{2}]\text{PF}_6$) with 50% probability ellipsoids.

13. Computational details

The DFT calculations were performed using Gaussian09¹⁵ software package. The B3LYP functional was used with the basis set 6-31G* for all non-nickel atoms and using the m6-31G* basis set for the nickel atom. This combination of hybrid functional and basis sets has been previously shown to work well for reproducing experimental parameters for Ni complexes.^{16,17} The use of triple-zeta basis sets (e.g., 6-311G*, tzvp, or def2tzvp) yielded very similar results and electronic transitions. Spin unrestricted geometry optimizations with a SCRF of acetonitrile were performed on $\mathbf{1}^+$, starting from the crystallographic coordinates with the counterions being excluded. The ground state wavefunction was investigated by analyzing the frontier MOs and the atomic contributions to frontier molecular orbital and calculated UV-Vis spectra were analyzed by the program Chemissian.¹⁸

Table S5. Cartesian coordinates for $[\text{Me}_4\text{N}4\text{Ni}^{\text{III}}\text{Cl}_2]^+(\mathbf{1}^+)$

Ni	0.00177300	-0.00131400	-0.00035500
Cl	2.24557400	0.00381700	0.02621500
N	-0.29789700	-0.29644600	2.17975000
N	-1.91793600	-0.15435600	-0.02463800
C	-4.60430500	-0.67523900	-0.05847400
C	-2.56637200	-0.28123900	1.14581500
C	-2.53664300	-0.28063000	-1.21115200
C	-3.90339300	-0.54358800	-1.25725000
C	-3.93382600	-0.54445000	1.15769300
H	-4.39815400	-0.64728700	-2.21696800
H	-4.45223500	-0.64885900	2.10474300
C	-1.74868200	-0.04253700	2.38938100
H	-1.86276700	1.01304800	2.65646500
H	-2.13870900	-0.63402500	3.22606400
C	-1.68811900	-0.04252800	-2.43417100
H	-1.79827800	1.01195600	-2.70723700
H	-2.05486700	-0.63734500	-3.27909000
N	-0.24241200	-0.29202400	-2.18700400
C	0.06819300	-1.71935400	2.41061300
H	-0.49789800	-2.14392300	3.24750100
H	1.12718700	-1.74685900	2.68796300
C	0.13427700	-1.71337300	-2.41070200
H	1.20076400	-1.73714000	-2.65814900
H	-0.40653000	-2.13766600	-3.26417800
C	-0.09430800	-2.56699000	1.17501500
C	-0.22835700	-3.94631000	-1.21499500
N	0.00325300	-1.92471300	-0.00169200

C	-0.26210000	-3.94922800	1.19985600
C	-0.32883200	-4.64095900	-0.00955900
C	-0.06146400	-2.56419900	-1.18212500
H	-0.34401500	-4.46320200	2.15149900
H	-0.28349700	-4.45801300	-2.16976900
H	-5.66861200	-0.88883500	-0.07200900
H	-0.46907800	-5.71743500	-0.01284000
Cl	-0.17348800	2.23528300	0.00255300
C	0.57317200	0.58669700	-3.05762300
H	0.38465500	0.36927900	-4.11753500
H	0.32041300	1.62723900	-2.84999700
H	1.62945100	0.42745500	-2.83647100
C	0.49772300	0.57818700	3.07278800
H	0.28173100	0.35919400	4.12709900
H	1.55878600	0.41624400	2.87807900
H	0.25335200	1.61985100	2.86060600

Table S6. Mulliken atomic spin densities for $[\text{MeN4Ni}^{\text{III}}\text{Cl}_2]^+$ (1^+)

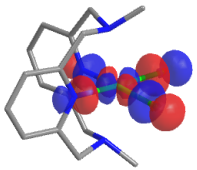
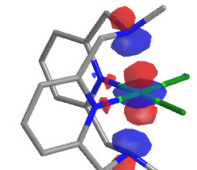
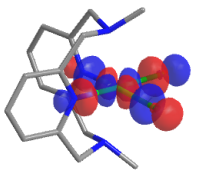
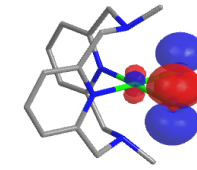
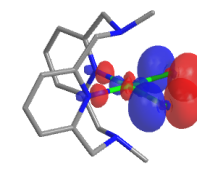
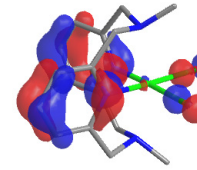
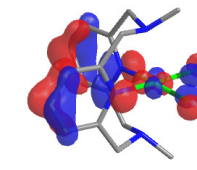
1 Ni	0.803743
2 Cl	-0.025843
3 N	0.120458
4 N	0.001985
5 C	-0.000675
6 C	-0.000030
7 C	-0.000021
8 C	-0.000921
9 C	-0.000919
10 H	0.000311
11 H	0.000311
12 C	-0.003375
13 H	0.000105
14 H	0.003991
15 C	-0.003362
16 H	0.000102
17 H	0.003993
18 N	0.120527
19 C	-0.003417
20 H	0.004005
21 H	0.000111
22 C	-0.003432
23 H	0.000112
24 H	0.004000
25 C	0.000022

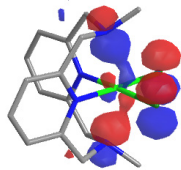
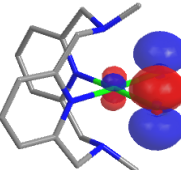
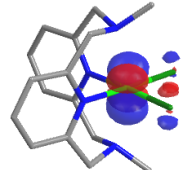
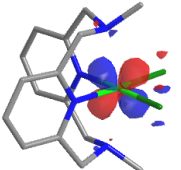
26	C	-0.000976
27	N	0.001208
28	C	-0.000976
29	C	-0.000625
30	C	0.000015
31	H	0.000300
32	H	0.000299
33	H	-0.000068
34	H	-0.000069
35	Cl	-0.026392
36	C	-0.006000
37	H	0.006359
38	H	0.001203
39	H	0.001192
40	C	-0.005999
41	H	0.006356
42	H	0.001197
43	H	0.001197

Table S7. Selected TD-DFT calculated vertical electronic excitation of $\mathbf{1}^+$ with oscillator strength.

Wavelength (nm)	Osc. Strength (<i>f</i>)	Major contributions
647.10	0.005	H-13(B)→L+1(B) (39%), HOMO(B)→L+1(B) (33%)
642.11	0.0019	H-1(A)→LUMO(A) (97%)
568.47	0.0039	H-5(A)→LUMO(A) (39%), H-4(B)→LUMO(B) (23%)
512.56	0.0025	H-4(A)→LUMO(A) (34%), H-3(B) →LUMO(B) (27%), H-12(B)→LUMO(B) (18%)
426.37	0.0076	H-9(A)→LUMO(A) (45%), H-5(A) →LUMO(A) (21%)
406.57	0.0185	H-8(A)→LUMO(A) (46%)
355.11	0.0027	H-10(A)→LUMO(A) (15%), H-8(B)→LUMO(B) (43%)
347.47	0.0053	H-11(A)→LUMO(A) (17%), H-8(A)→LUMO(A) (45%)
338.52	0.0822	H-13(B)→L+1(B) (18%), HOMO(B)→L+1(B) (44%)
322.46	0.0178	H-14(A)→LUMO(A) (18%), H-12(B)→LUMO(B) (43%)
321.07	0.0452	H-10(A)→LUMO(A) (31%), H-4(B)→LUMO(B) (17%)
320.92	0.0048	HOMO(A)→L+1(A) (15%)
317.55	0.0029	HOMO(A)→L+1(A) (75%)
310.89	0.0016	H-8(B)→L+1(B) (42%), H-4(B)→L+1(B) (21%)
302.05	0.0036	H-5(B)→L+1(B) (34%)
298.67	0.0014	H-5(B)→L+1(B) (42%)

Table S8. Atomic contributions of molecular orbitals for complexes 1^+ . Orbitals associated with the transitions of interest (406, 426, 512, 647 nm) are shown. Only atoms interacting with Ni are shown.

MO #	MOs (0.05 isocontour value)	Ni	2N (ax.)	2N (eq.)	2Cl
1^+ α -LUMO (104 α)		44	0	20	30
1^+ β -LUMO+1 (104 β)		67	18	4	4
1^+ β -LUMO (103 β)		56	0	16	22
MO #	MOs (0.05 isocontour value)	Ni	2N (ax.)	2N (eq.)	2Cl
1^+ α -HOMO-4 (99 α)		6	0	0	89
1^+ α -HOMO-5 (98 α)		8	0	6	82
1^+ α -HOMO-8 (95 α)		0	0	30	14
1^+ α -HOMO-9 (94 α)		12	0	22	13

1^+ β -HOMO (102 β)		11	36	0	36
1^+ β -HOMO-3 (99 β)		9	0	0	84
1^+ β -HOMO-12 (90 β)		87	0	0	9
1^+ β -HOMO-13 (89 β)		83	2	0	9

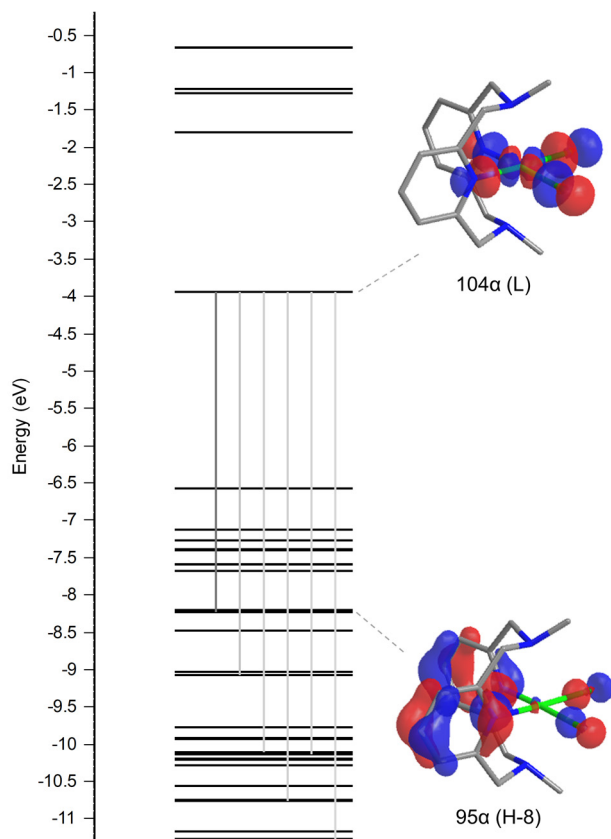


Figure S23. Frontier molecular orbital (α -MO) diagram for 1^+ corresponding to 406.57 nm excitation as determined by TD-DFT computation.

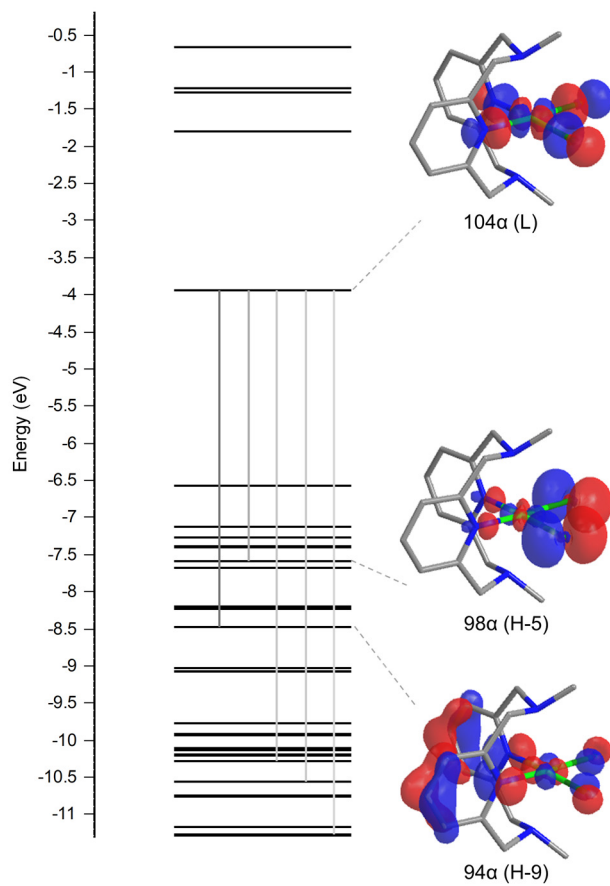


Figure S24. Frontier molecular orbital (α -MO) diagram for 1^+ corresponding to 426.37 nm excitation as determined by TD-DFT computation.

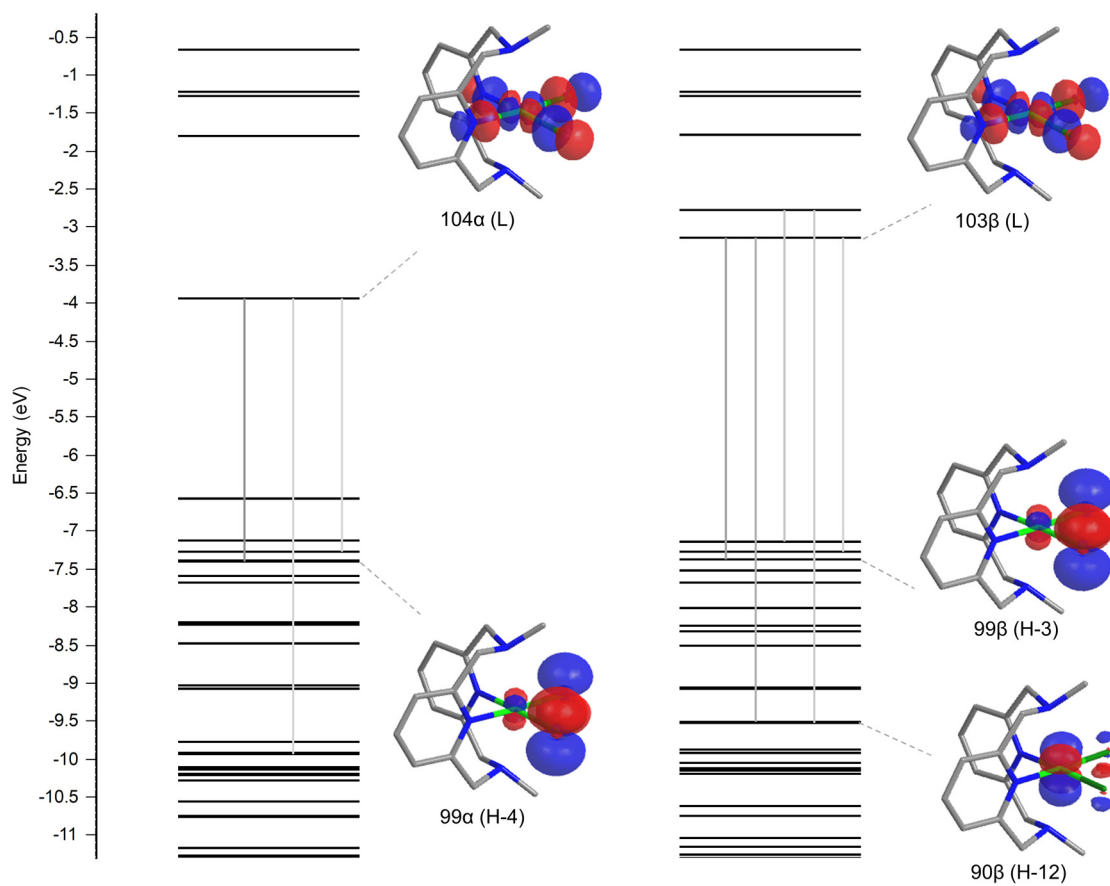


Figure S25. Frontier molecular orbital (α -MO (left) and β -MO (right)) diagram for 1^+ corresponding to 512.56 nm excitation as determined by TD-DFT computation.

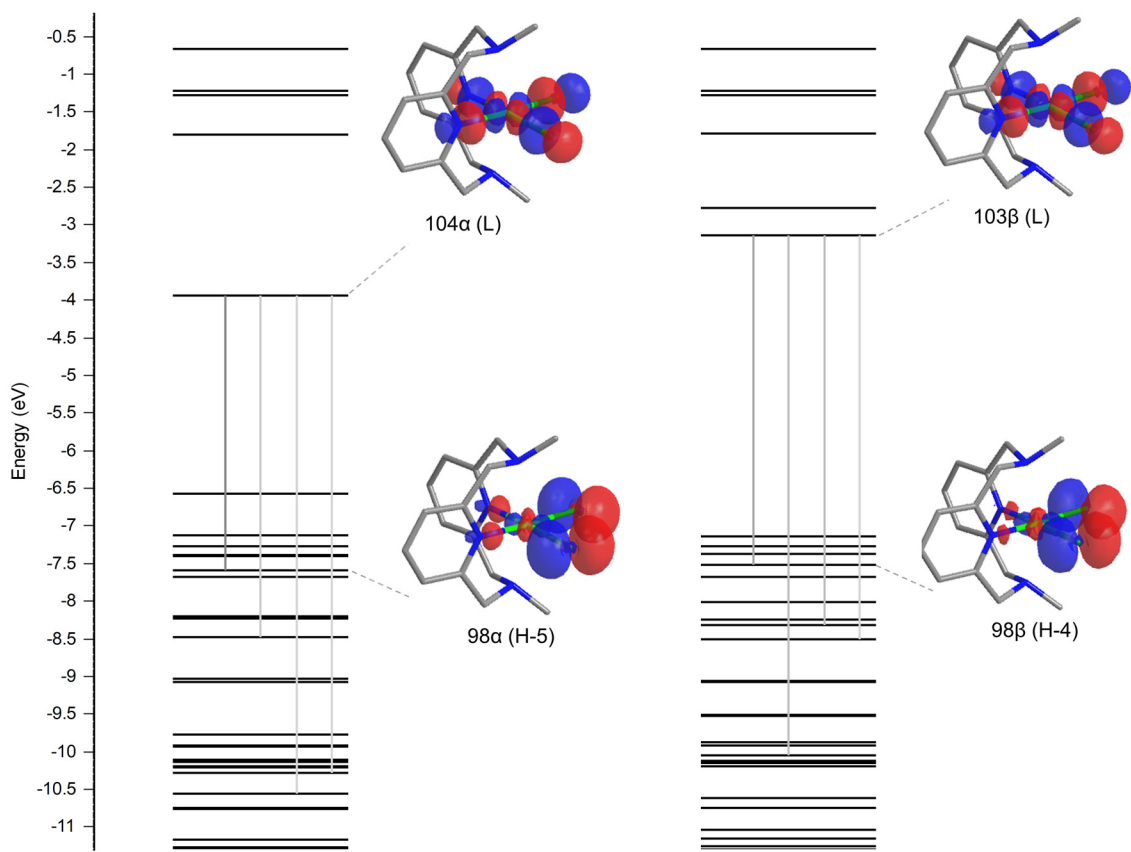


Figure S26. Frontier molecular orbital (α -MO (left) and β -MO (right)) diagram for 1^+ corresponding to 568.48 nm excitation as determined by TD-DFT computation.

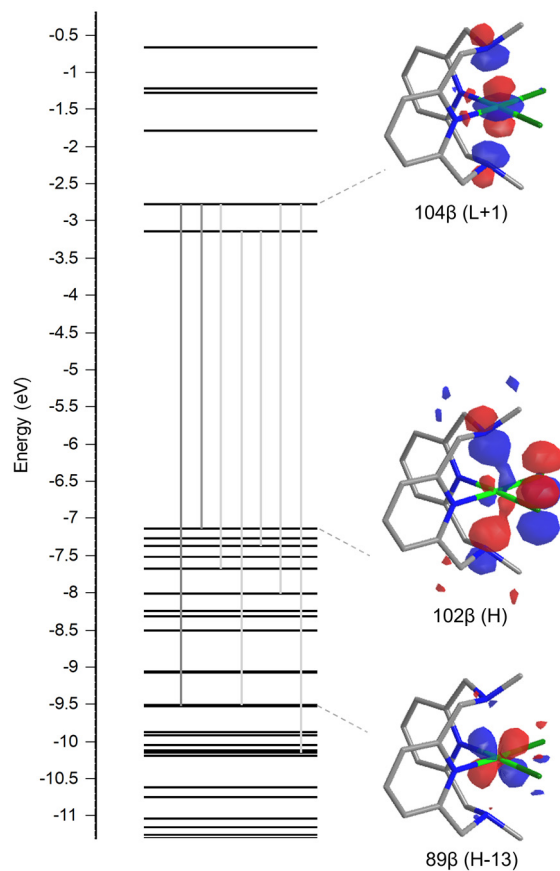


Figure S27. Frontier molecular orbital (β -MO) diagram for 1^+ corresponding to 647.10 nm excitation as determined by TD-DFT computation.

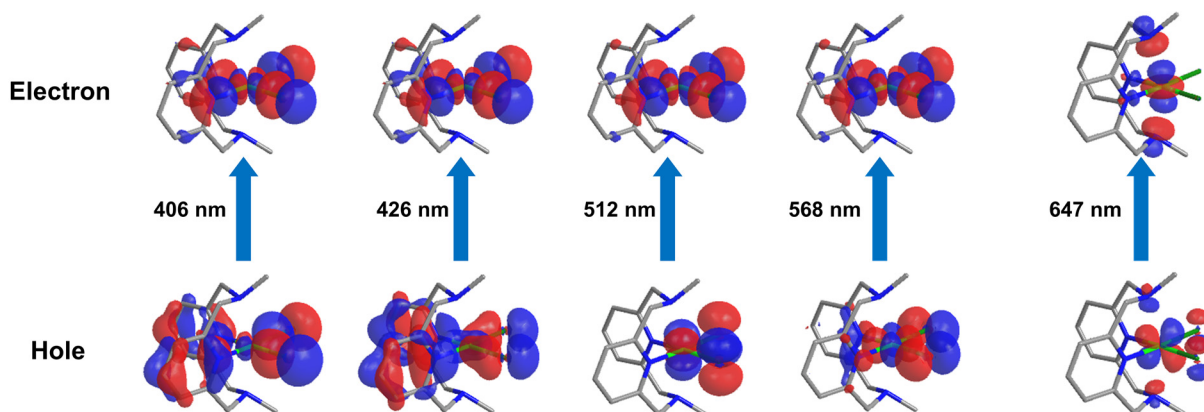


Figure S28. Natural transition orbitals (NTOs) analysis of the transitions.

14. References

1. D. F. Evans, *J. Chem. Soc.*, 1959, 2003.
2. J. Loliger, R. Scheffold, *J. Chem. Educ.*, 1972, **49**, 646.
3. A. Zielinska, L. Skulski, *Tetrahedron Lett.*, 2004, **45**, 1087.
4. B. Boduszek, H. J. Shine, *J. Org. Chem.*, 1988, **53**, 5142.
5. F. Bottino, M. Di Grazia, P. Finocchiaro, F. R. Fronczek, A. Mamo, S. Pappalardo, *J Org Chem*, 1988, **53**, 3521.
6. H. J. Kuhn, S. E. Braslavsky, R. Schmidt, *Pure Appl. Chem.*, 2004, **76**, 2105.
7. C. G. Hatchard, C. A. Parker, E. J. Bowen, *Proc. Royal Soc. London A, Math. Phys. Sci.*, 1956, **235**, 518.
8. C. A. Parker, E. J. Bowen, *Proc. Royal Soc. London A, Math. Phys. Sci.*, 1953, **220**, 104.
9. T.-P. Lin, F. P. Gabbai, *J. Am. Chem. Soc.*, 2012, **134**, 12230.
10. Y. Kotake, K. Kuwata, *Bull. Chem. Soc. Jpn.*, 1981, **54**, 394.
11. G. R. Buettner, *Free Radic. Biol. Med.*, 1987, **3**, 259.
12. G. Sheldrick, *Acta Cryst. Sec. A*, 2015, **71**, 3.
13. Bruker, *Madison, Wisconsin, USA*, 2018.
14. L. Krause, R. Herbst-Irmer, G. M. Sheldrick, D. Stalke, *J. Appl. Crystallogr.*, 2015, **48**, 3.
15. G. W. T. M. J. Frisch, H. B. Schlegel, G. E. Scuseria, M. A. Robb, J. R. Cheeseman, G. Scalmani, V. Barone, B. Mennucci, G. A. Petersson, H. Nakatsuji, M. Caricato, X. Li, H. P. Hratchian, A. F. Izmaylov, J. Bloino, G. Zheng, J. L. Sonnenberg, M. Hada, M. Ehara, K. Toyota, R. Fukuda, J. Hasegawa, M. Ishida, T. Nakajima, Y. Honda, O. Kitao, H. Nakai, T. Vreven, J. A. Montgomery, Jr., J. E. Peralta, F. Ogliaro, M. Bearpark, J. J. Heyd, E. Brothers, K. N. Kudin, V. N. Staroverov, R. Kobayashi, J. Normand, K. Raghavachari, A. Rendell, J. C. Burant, S. S. Iyengar, J. Tomasi, M. Cossi, N. Rega, J. M. Millam, M. Klene, J. E. Knox, J. B. Cross, V. Bakken, C. Adamo, J. Jaramillo, R. Gomperts, R. E. Stratmann, O. Yazyev, A. J. Austin, R. Cammi, C. Pomelli, J. W. Ochterski, R. L. Martin, K. Morokuma, V. G. Zakrzewski, G. A. Voth, P. Salvador, J. J. Dannenberg, S. Dapprich, A. D. Daniels, O. Farkas, J. B. Foresman, J. V. Ortiz, J. Cioslowski, D. J. Fox., *Gaussian 09, Revision A.02*, Gaussian, Inc., Wallingford CT, 2009.
16. C. M. Lee, C. H. Chen, F. X. Liao, C. H. Hu, G. H. Lee, *J. Am. Chem. Soc.*, 2010, **132**, 9256.
17. C.-P. Zhang, H. Wang, A. Klein, C. Biewer, K. Stirnat, Y. Yamaguchi, L. Xu, V. Gomez-Benitez, D. A. Vicic, *J. Am. Chem. Soc.*, 2013, **135**, 8141.
18. Chemissian, version 4.60, 2018, www.chemissian.com, accessed June 2019.